IEEE Robotics and Automation Letters (RAL) paper presented at the
2020 IEEE International Conference on Robotics and Automation (ICRA)
31 May - 31 August, 2020. Paris, France

Backdrivable and Fully-Portable Pneumatic Back Support Exoskeleton for Lifting Assistance

Ung Heo, Sangjoon J. Kim and Jung Kim, *Member, IEEE*

***Abstract*— To reduce the possibility of lower back pain (LBP), which is the most frequent injury in manual labor, several back support exoskeletons have been developed and implemented for lifting motion assistance. Although pneumatic power transmission is attractive due to its inherent compliance and backdrivability, the portability of the pneumatic system is highly limited due to the bulky air compressors that provide compressed air to the system. Therefore, we aimed to develop a fully-portable pneumatic back support exoskeleton by integrating all pneumatic components in the system. The compressed air consumption and generation of pneumatic system were modeled to meet design requirements. The developed exoskeleton was completely stand-alone and provides 80 Nm of maximum extension torque for 6 liftings per minute (6 l/m). The upper limit of the resistance torque was estimated to be about 2 Nm, which implies high backdrivability. Finally, lifting experiments were performed and surface electromyography (sEMG) was measured to validate the physical assistance of the developed exoskeleton system for ten subjects. Compared to the case with no exoskeleton, the back muscle activation was significantly reduced with the assistances.**

I. Introduction

Manual laborers in the industrial workplaces suffer from work-related musculoskeletal disorders (WMSD), which not only deteriorate individual quality of life but also incur great economic and social costs [1], [2]. Industrial exoskeletons have the potential to reduce physical load and the risk of WMSD by assisting laborers [3]. The most frequent WMSD in manual labor is lower back pain (LBP) [4], [5]. For this reason, most currently developed industrial exoskeletons are intended to support the back during tasks with high risk of LBP, such as lifting, lowering and static bending [3].

Depending on the actuation type, powered back support exoskeletons are generally categorized as either electric motor-driven or pneumatic-driven. Commercial powered back support exoskeletons are generally of electric motor-driven type, except for the Muscle Suit [6]-[8]. Motor-driven systems generally have the characteristic of being fully portable, which is an important advantage for industrial exoskeletons in a dynamic workplace. However, to amplify the low output torque of electric motor-driven actuators, a gearbox with high reduction ratio must be installed, which causes high mechanical impedance due to amplified friction and inertia. Consequently, electric motor-driven systems are vulnerable to impact and this reduces backdrivability, which has disadvantages on user safety and comfort [9].

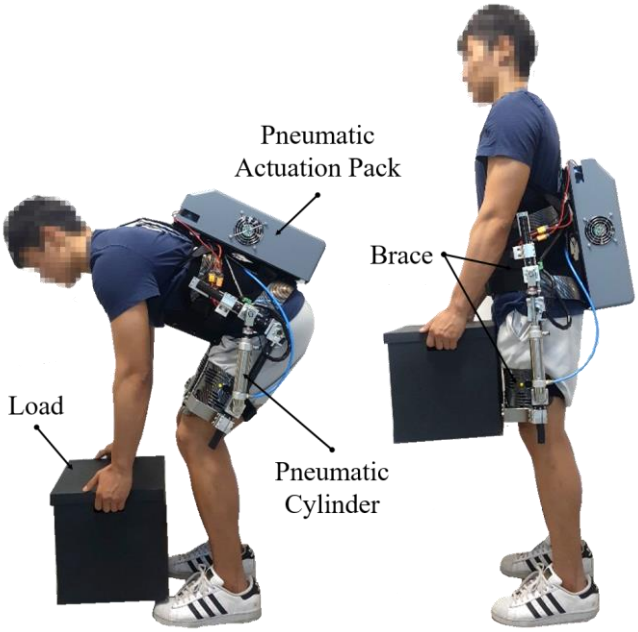

Fig. 1. System overview of a portable pneumatic back support exoskeleton. The system is powered by a pneumatic cylinder and fully portable due to a microcompressor inside a pneumatic actuation pack.

On the other hand, pneumatic-driven systems have considerable advantages for wearable robotic applications because they are backdrivable and conducive for human use due to the inherent compressibility of the air, which implies safe and comfortable physical human-robot interaction in wearable robotics [10]. Also, pneumatic-driven systems are more robust than software-rendered compliance and backdrivability systems under malfunction and power failure [9]. However, conventional pneumatic back support exoskeletons, including several laboratory prototypes [11], [12], require large air compressors, which significantly limits their portability, and thus the practicality of the system [10], [13]. This study therefore aims to design a portable pneumatic actuation system for back support exoskeleton application.

There have been efforts to develop portable pneumatic sources [14]-[21]. According to previous studies, electric motor-based microcompressors are suitable for wearable applications because they are easily adaptable to battery-powered systems and involve no potential hazards [20]. Therefore, in this study, we customized and applied a previously developed microcompressor for back support application [21]. Since the portable pneumatic sources has

This work was supported by the Bio & Medical Technology Development Program of the National Research Foundation (NRF) funded by the Korean government (MSIT) (No. NRF-2017M3A9E2063103). (Corresponding author: Jung Kim.)

The authors are with the Department of Mechanical Engineering, Korea Advanced Institute of Science and Technology, Daejeon 305-701, South Korea (e-mail: ksgjdnd@kaist.ac.kr; sangjoon.j.kim@kaist.ac.kr; jungkim@kaist.ac.kr)

limited flow rate compared to large conventional compressors, we used a reservoir to increase the pressure by accumulating compressed air from the microcompressor. In this study, the design requirements for portability and performance for lifting assistance were defined based on previous studies. Then, the actuation mechanism was designed and its backdrivability was experimentally verified. The reservoir and microcompressor were designed by pressure dynamics modeling to meet the design requirements. The total weight of the developed system is about 9.2 kg and the battery (750 g) was able to power lifting assistance for 1.6 hour. Finally, the physical effectiveness of the developed system was shown by reduced back muscle activation.

In Section II, the overall mechanical structure and performance of the designed mechanism are presented. In Section III, the pneumatic system design method based on pressure dynamics modeling is presented. In Section IV, lifting experiments are used to evaluate the performance of the system in terms of back muscle activation. Section V presents a discussion of results, concludes the paper and provides information on future work.

II. Structural Design

It has been reported that, to be portable, exoskeletons worn on the torso must have weights of less than 15 % of the weight of the wearer [22]. In this study, the maximum weight limit of the whole system is set at 10.5 kg, assuming that the weight of the wearer is about 70 kg.The configuration of the system is shown in Fig. 1. The human body and exoskeleton are in contact with a commercial trunk/thigh brace and shoulder strap. For user's safety and comfort, braces and strap disperse the weight and interaction force exerted on the skin. Also, each brace position can be adjusted to fit different body sizes. As can be seen in Fig. 2, there is a single degree of freedom (1 DoF) rotational joint between the upper and lower link and a pneumatic cylinder is connected between them on each side. A pair of cylinders (CM2D32-75FZ, SMC, Japan) with diameter of 32 mm and stroke of 75 mm was selected as the actuator. The estimated joint torque on the lower back is about 240 Nm when lifting a 15 kg object and a target torque of 80 Nm, which is about a third of the joint torque, is suggested as sufficiently strong [23]-[26]. Therefore, a peak assistance torque of 80 Nm is aimed at in this study.

The moment arm of the force induced by the cylinders varies with respect to the trunk flexion. Higher torque can be obtained with a constant actuation force and larger flexion angle due to the increased moment arm. When the user is in the upright position, both the required torque and the moment arm becomes zero, a situation that is safe and efficient.

Equation (1) is the dynamic equation of the cylinder. M_p is the mass of the piston-rod assembly. F is the force exerted by the cylinder rod. x is the position of the piston from the lowest point of the cylinder stroke; P_a, P_b are the pressure of chambers a and b, respectively. A_a, A_b and A_r are the cross-sectional area of each chamber and of the piston rod. β is the viscous friction coefficient and F_f is the Coulomb friction force [27].

$$M_p\ddot{x} + \beta\dot{x} + F_f sign(\dot{x}) = P_a A_a - P_b A_b - P_{atm} A_r - F \quad (1)$$

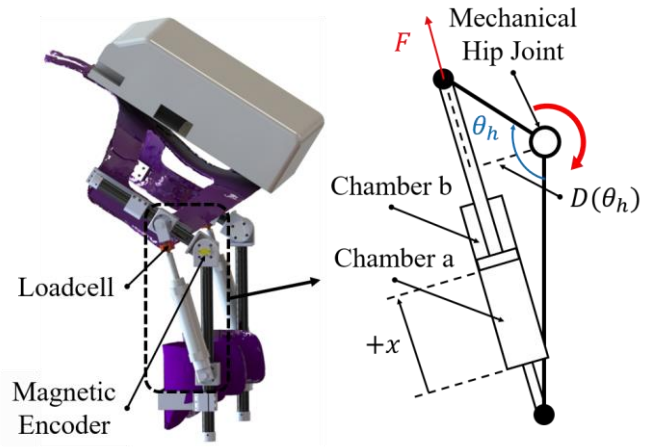

Fig. 2. Mechanical configuration and modeling of developed system.

It is assumed that M_p is negligibly small. Since lifting requires unidirectional assistance, the opposite cylinder chamber is always kept at atmospheric pressure, because no air supply is required ($P_b = P_{atm}$). The cross-sectional area of chamber a equals to sum of cross-sectional area of chamber b and piston rod ($A_a = A_b + A_r$). Therefore, (1) can be written as (2)

$$F = (P_a - P_{atm})A_a - \beta\dot{x} - F_f sign(\dot{x}) \quad (2)$$

The total output torque for both cylinders can be expressed in (3). θ_h is the hip joint angle; $D(\theta_h)$ is the moment arm of the mechanism, which is a function of θ_h. τ is the torque resulting from both cylinders to the upper link.

$$\tau = 2FD(\theta_h) \quad (3)$$

The transparent mode refers to a control strategy for zero human-exoskeleton interaction torque. High backdrivability implies low interaction torque in transparent mode. In this study, to achieve transparency, the cylinder chamber pressure was simply kept at atmospheric pressure. Therefore, in transparent mode, the frictional force f and the resulting resistance torque τ_f from the mechanism are described in (4)

$$\begin{cases} f = -\beta\dot{x} - F_f sign(\dot{x}) \\ \tau_f = 2fD(\theta_h) \end{cases} \quad (4)$$

τ_f is a function of θ_h and $\dot{\theta_h}$, as shown in (4). The frictional parameters of cylinder (β, F_f) were identified with an experiment. The cylinder was perturbed manually with range of linear speed (-0.3~0.3 m/s) and the frictional force was measured. The relationship between frictional force and cylinder speed is shown in Fig.3. According to the experiments in the previous study, the average hip joint angular velocity ($\dot{\theta_h}$) during fast lifting is about 130 °/s [28]. Based on the identified parameters and lifting speed, the possible peak τ_f is estimated about 2 Nm, which is less than 1 % of lifting joint torque [25], thus implies the developed mechanism has high backdrivability under fast moving condition (130 °/s). Thus, in most situations we can assume

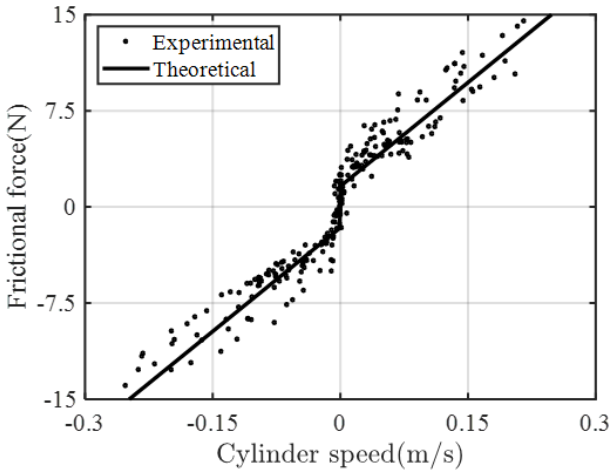

Fig. 3. Model parameters of friction force were identified. The experimental data points are plotted according to cylinder speed ($\dot{x}$) in red dots and the black line is the fitted result ($\beta = 54.0,\ F_f = 1.62,\ R^2 = 0.953$).

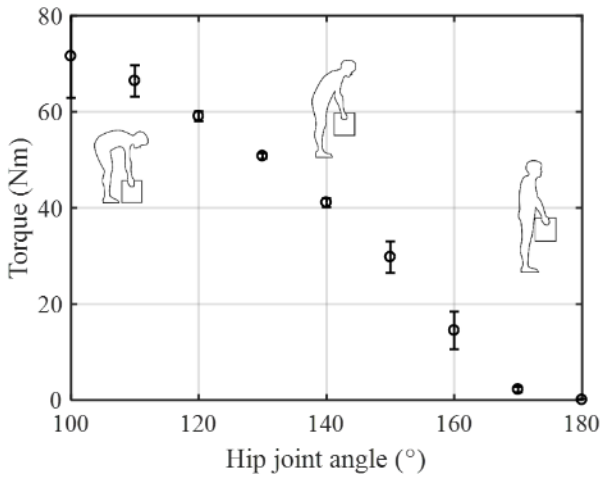

Fig. 4. Ensemble averaged measured output torque with respect to θ_h for 6 lifting trials with different lifting speeds. The errorbar represents ± 1 standard deviation across trials.

that τ_f is small enough to be ignored. The pressure required to achieve the target torque of 80 Nm with the selected cylinder is 700 kPa and the measured torque profile with respect to θ_h at 700 kPa is shown in Fig. 4. A total of 6 lifting trials ($\dot{\theta_h}$=64.4±9.6 °/s) were performed and the measured interaction torques were the ensemble averaged with respect to θ_h . Thus, the designed mechanism satisfied the backdrivability and torque design requirements.

Active back support exoskeletons have various sensors to control the system by utilizing kinetic and kinematic data [26], [28]. As shown in Fig. 2, the load cells (CDF40-100, Bongshin Loadcell, Rep. of Korea) are connected in series with the cylinder rod to measure the force from the cylinder rod to each link and absolute rotary magnetic encoders (SME360C, SERA, Rep. of Korea) are attached to measure the angle of the hip joint. Inside the pneumatic actuation pack, as shown in Fig. 6, pressure sensors (ISE30A-01, SMC, Japan) are used to measure the pressure of the reservoir and cylinders. A controller (myRIO-1900, National Instruments, USA) is implemented that communicates remotely with the host PC via Wi-Fi; data sampling frequency is 1 kHz. The entire system was powered by an embedded Li-ion battery.

III. Portable Pneumatic System Design

The working principle of the proposed pneumatic system is shown in Fig. 5. Compressed air generated from microcompressor is accumulated in the reservoir. Regulator controls the cylinder pressure.

The maximum acceptable lifting frequency range at the worksite is approximately 6 liftings per minute (6 l/m), so this is defined as the nominal target frequency [29]. Also, we aimed at a reservoir capacity sufficient to support continuous actuation twice instantaneously without generating compressed air by using air accumulated in the reservoir.

Fig. 6 shows the configuration of the pneumatic system. The microcompressor generates compressed air, which is accumulated in the reservoir and transported to the cylinder through the pressure regulator. A 3-way proportional pressure

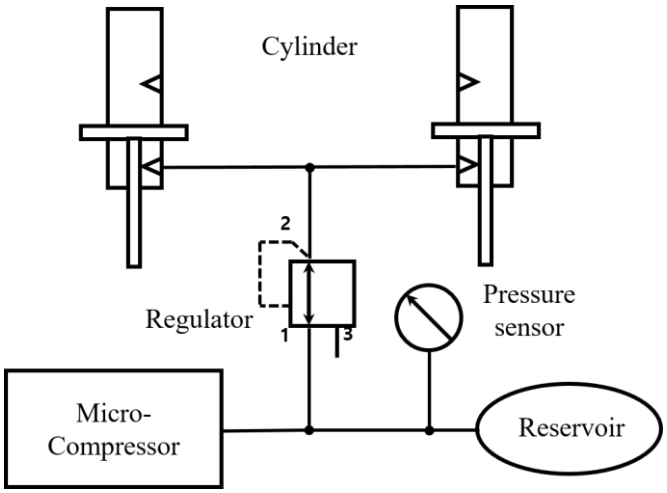

Fig. 5. Pneumatic circuit diagram of proposed system.

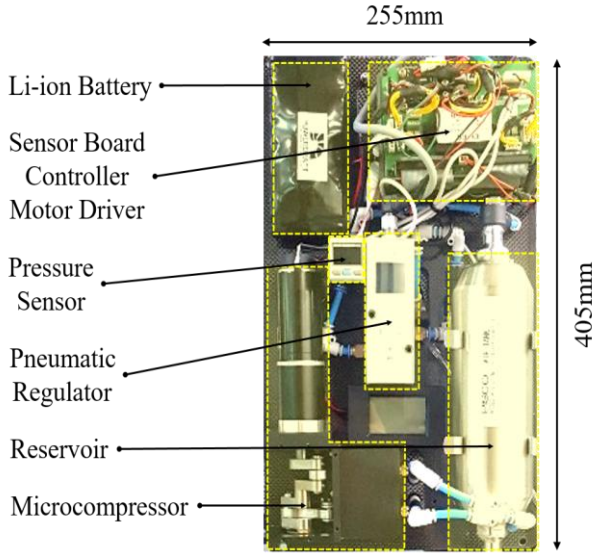

Fig. 6. Components inside the pneumatic actuation pack for generation, accumulation and control of compressed air.

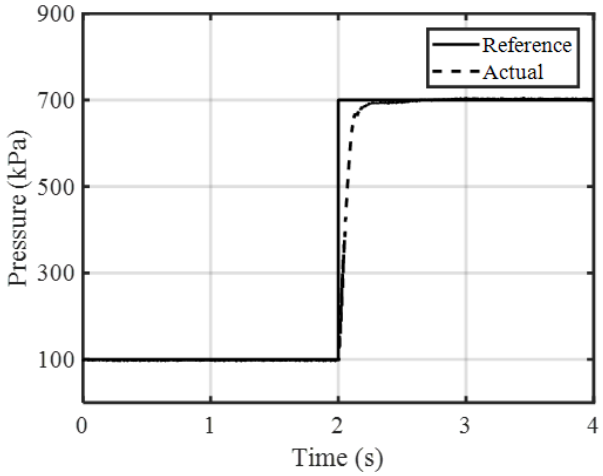

Fig. 7. Reference step input (700 kPa) and actual pressure trajectory. The 10% to 90% rise time is about 100ms.

regulator (VPPM-6L, Festo, Germany) was selected to control pressure of cylinder chamber. The pressure regulator controls the output pressure by comparing the desired pressure with the actual pressure through internal feedback control [30]. Fig. 7 shows reference step input (700kPa) and measured cylinder pressure trajectory controlled by the pressure regulator.

A. Air Consumption Modeling for Reservoir Design

The following assumptions were applied: 1) air is an ideal gas, 2) the temperature of the chamber and the reservoir are uniformly distributed, 3) the potential and kinetic energy are ignored and 4) an adiabatic process is assumed. By the ideal gas law, continuity equation and energy equation, the pressure dynamics equation of the control volume can be written as (5) [27]

$$\dot{P} = k\frac{RT}{V}\dot{m} - k\frac{P}{V}\dot{V} \tag{5}$$

P, T and V are pressure, temperature and volume of the control volume. k is specific heat ratio, R is gas constant of air and $\dot{m}$ is the mass flow rate. Equation (5) is applied to the reservoir and the cylinder and can be written as (6). Subscript a means cylinder and r means reservoir.

$$\begin{cases} \dot{P}_a = k\dfrac{RT}{V_a}\dot{m}_a - k\dfrac{P_a}{V_a}\dot{V}_a \\ \dot{P}_r = k\dfrac{RT}{V_r}\dot{m}_r \end{cases} \tag{6}$$

Air flow during lifting is assumed only from the reservoir to the cylinder and no leakage occurs. Then, the relationship between the mass flow rate of the reservoir and cylinder during lifting can be described by (7)

$$\dot{m}_r = -\dot{m}_a \tag{7}$$

Cylinder pressure change during lifting can be divided into two steps. In the first step, it is assumed that the change of the cylinder chamber volume is 0 ($\dot{V}_a = 0$) in the pressure rising period since the time to reach desired pressure is sufficiently fast (about 0.2 s); it is assumed that there is no displacement of the cylinder due to lifting. The second step assumes an ideal isobaric expansion process ($\dot{P}_a = 0$).

By ignoring the cylinder pressure ripple, it was assumed that the pressure was controlled by the regulator at 700 kPa of constant pressure during lifting. The pressure drop of the reservoir for each step can then be obtained as (8) by integrating (6) and (7) with respect to time.

$$\begin{cases} \Delta P_{r1} = -\frac{V_0}{V_r}\Delta P_a \\ \Delta P_{r2} = -kP_{a,des}\frac{\Delta V_a}{V_r} \\ \Delta P_{r,total} = \Delta P_{r1} + \Delta P_{r2} \end{cases} \tag{8}$$

ΔP_{r1} and ΔP_{r2} are the pressure drop of the reservoir during each step. ΔP_a is the cylinder pressure change (600 kPa in this case) and $P_{a,des}$ is the desired constant cylinder pressure (700 kPa in this case). ΔV_a is the cylinder volume change under full-stroke actuation and V_0 is the dead volume of the cylinder including pneumatic tubing. $\Delta P_{r,total}$ is the total change of reservoir pressure. Based on (8), the minimum reservoir pressure required to actuate the cylinder at the desired pressure of 700 kPa can be determined. Therefore, the desired reservoir pressure for n times actuations at 700 kPa can be obtained as (9)

$$P_{des,n} = P_{a,des} + n\Delta P_{r,total} \tag{9}$$

Fig. 8 shows $P_{des,n}$ according to the reservoir volume. Since the maximum output pressure of the microcompressor is theoretically 1100 kPa, to assist twice (n = 2) continuously from a fully charged reservoir, the volume of the reservoir should be greater than 0.65 L ($V_{r,min}$). The larger the volume of the reservoir, the more stably the air can be supplied [13], but the lower the portability due to device volume and weight. Thus, the smaller reservoir should be used as long as it satisfies the desired performance. Therefore, a 0.75 L commercial reservoir (PISCO, ATS-0.75, USA) was used in

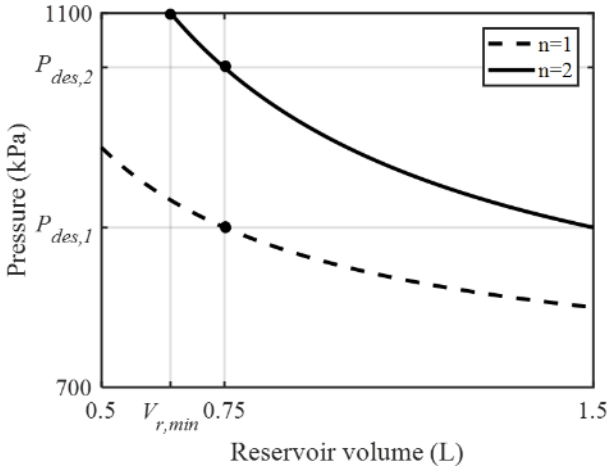

Fig. 8. Desired reservoir pressure ($P_{des,n}$) to volume of reservoir (V_r). For example, to actuate the cylinder twice (n = 2) with fully charged reservoir, the volume of the reservoir should be at least 0.65 L (=$V_{r,min}$).

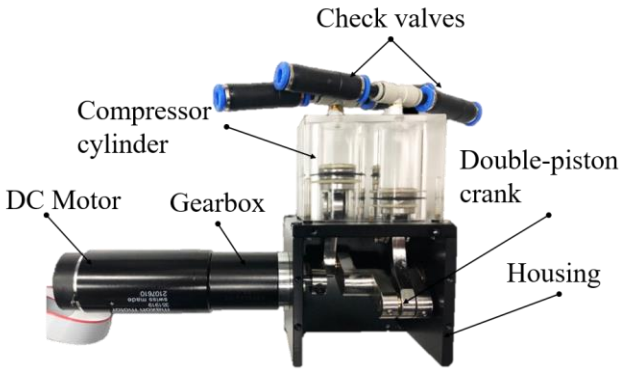

Fig. 9. Structure of customized microcompressor. Ambient air is compressed via double piston crank mechanism.

this study. However, with the selected reservoir, the actual measured $\Delta P_{r,total}$ was about 190 kPa and the value calculated from (8) was about 170 kPa, which is about 10.5% of modeling error. This is because modeling includes ideal assumptions and does not take into account additional pressure drop due to energy loss and leakage. Therefore, when designing the microcompressor, 890 kPa and 1080 kPa were used as $P_{des,1}$ and $P_{des,2}$ respectively, by considering the actual measured values of the pressure drop.

B. Microcompressor Design

The overview of the microcompressor is shown in Fig. 9. It is designed to generate 1100 kPa of maximum pressure with a double-piston crank mechanism driven by a DC motor-gearbox [21]. In this study, the main concept of the design was to achieve identical maximum pressure; however, the DC motor-gearbox module was changed to increase the flow rate for lifting assistance application.

$$P_i = (P_{max} - P_{i-1})\frac{V_c}{V_c + V_{sys}} + P_{i-1} \quad (10)$$

The relationship between the design variables of the microcompressor is described in (10) [21]. P_i is the pressure of the reservoir in the i th stroke, P_{max} is the maximum pressure of the compressor, V_c is the volume of the compressor cylinder when the compressor piston is fully compressed and V_{sys} is the total volume including the reservoir and pneumatic tubing.

A DC motor with a planetary gearbox 26:1 (RE40, Maxon, Switzerland), for which the nominal torque is 4.6 Nm and nominal speed is 267 rpm, were selected to meet the design requirements. Fig. 10a shows the experimental validation of the designed microcompressor and reservoir. The cylinder is actuated at 6 l/m of frequency with 700 kPa of pressure, and the microcompressor generates compressed air to maintain the reservoir pressure at $P_{des,1}$ (890 kPa). Fig. 10b shows that when the reservoir is charged at $P_{des,2}$ (1080 kPa) of pressure, the cylinder can be actuated twice at 700 kPa without supplying compressed air from the microcompressor. Therefore, the designed reservoir and microcompressor satisfy the design requirements.

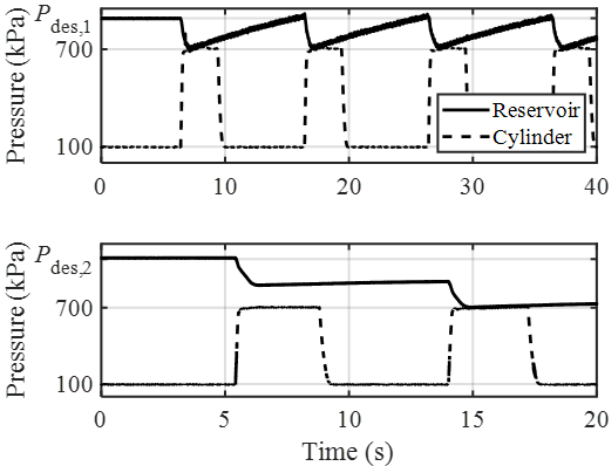

Fig. 10. Reservoir and cylinder pressure under continuous lifting assistance (6 l/m) (a) and assist twice with fully-charged reservoir and without generating compressed air (b).

IV. Experimental Evaluation

To investigate the effect of the developed exoskeleton on muscle activity during lifting, muscle activation measurement experiments were conducted with wireless surface electromyography (sEMG) sensors (Trigno system, Delsys, USA). The sampling frequency was 2 kHz.

Ten males (age of 22.3±1.7 years, height of 1.71±0.04 m and weight of 69.5±5.0 kg) who had no experience of LBP were the volunteers. The hip joint of the wearer and the exoskeleton were aligned by adjusting the brace location before the experiment. Experimental setup is shown in Fig. 11a. The movement started from the upright posture, with trunk bending, grasping and lifting of a box on the ground, and then a return to upright posture. The box size was 35×29×18 cm and it was located 30 cm of height from the ground. The lifting was performed during one minute at a frequency of 6 l/m and it was synchronized with actuation frequency.

A visual feedback displayed in a monitor provided timing information to user when to start lowering and lifting. Lowering cue was provided 5 seconds before lifting cue.

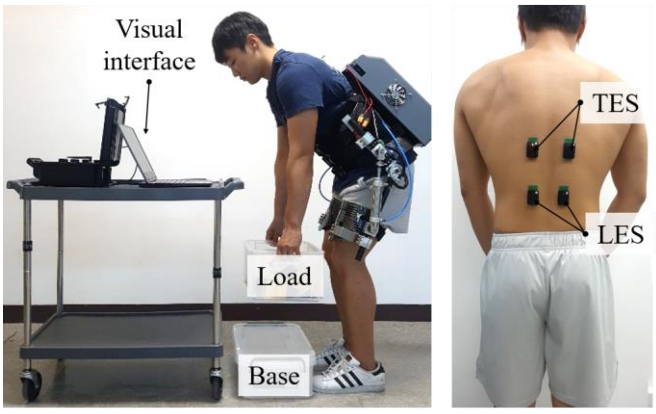

Fig. 11. Experimental setup (a) and sEMG electrode placement for TES and LES muscles (b).

Subjects were instructed to not start lifting before the assist was provided. Since the assist was strong enough to be recognized by the user and to initiate the user's movement, motion and assist moment were able to synchronyzed.

Subjects performed lifting of two different weights (10 kg and 20 kg), without the exoskeleton and with the exoskeleton (noExo, Exo-On). Following SENIAM guidelines [31], sEMG electrodes were attached to the thoracic erector spinae (TES) at the T9 level and lumbar erector spinae (LES) at the L4 level, as shown in Fig. 11b [32]. The experimental protocol was approved by the Institutional Review Board of Korea Advanced Institute of Science and Technology (KAIST). Written informed consent and assent were obtained from each participant.

EMG data during lifting were normalized to the maximal voluntary contraction (MVC) of each muscle previously measured before the experiment. The raw EMG signals were low pass filtered using a second order Butterworth filter with 2.7 Hz cutoff frequency after rectification [33]. Then, each lifting trial was normalized by entire lifting time (%Lifting) for each subject. The normalized muscle activities of each subject were ensemble averaged across the subjects for each condition. The normalized muscular activity data were averaged with respect to the lifting cycle. The mean normalized EMG of each muscle was used as a dependent variable for the statistical analysis. Paired-samples t-tests with significance level of 0.05 were performed to investigate the effect of exoskeleton for each weight condition on back muscle activity.

The results of the experiments are shown in Fig. 12 and Fig. 13. The ensemble-averaged normalized muscular activity values across all subjects for each condition are shown in Fig. 12. The red and blue lines are the mean muscular activity of the 'noExo' and 'Exo-On' conditions, respectively. The shaded area represents ±1 standard deviation (SD) across all subjects.

The EMG values of both muscles for each condition are shown in Fig. 13. For both '10 kg' and '20 kg' conditions, significant reductions of EMG for both muscles were observed. For '10 kg', the EMG decreased 18.3% (TES) and 25.5% (LES) ($p<0.012$, $p<0.016$) and for '20 kg', it decreased 18.7% (TES) and 24.7% (LES) ($p<0.005$, $p<0.008$)

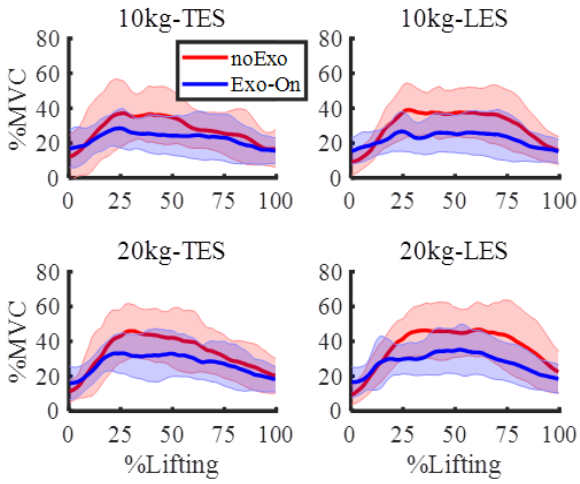

Fig. 12. Muscle activities (%MVC) with respect to lifting cycle (%Lifting) for each muscle (TES/LES) with respect to noExo/Exo and 10 kg /20 kg conditions.

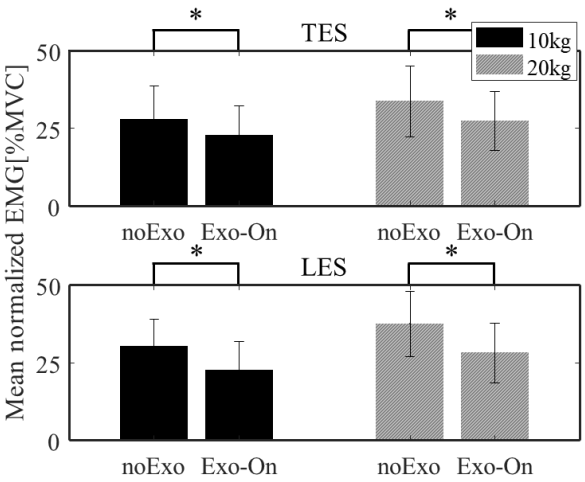

Fig. 13. Mean normalized EMG of TES and LES were reduced with exoskelton compared to noExo conditions.

V. Discussion and Conclusion

This study aimed to develop a back support exoskeleton with high backdrivability and provide a design method of a portable pneumatic system for specific performance requirements. In the transparent mode of the developed mechanism, the resistance torque introduced by the frictional force of the cylinder was identified, so that about 2 Nm of maximum resistance torque was estimated, which is less than 1% of lifting joint torque, therefore implying that the developed mechanism is highly backdrivable.

The microcompressor was used as a pneumatic source for the fully-portable pneumatic actuation system. By modeling the compressed air consumption, generation of microcompressor and the reservoir that stores the air, the pneumatic system was designed to meet the design requirements, providing a desired pressure of 700 kPa in 6 l/m frequency. However, about 10.5 % of error occurred in the compressed air consumption modeling due to energy loss in the empirical situation, which is not considered in the simplified model. This is expected to improve with the use of more precise models in future work. In addition, to examine the feasibility of suggested system, instead of implementing a specific assistive strategy, 80 Nm of peak torque was provided by maintaining a constant pressure of 700 kPa during lifting assist. In future work, we will implement a more advanced assistive strategy for lifting assistance and design the pneumatic system accordingly.

Experiments were conducted to verify the effectiveness of the physical assistance of the developed system by measuring the muscular activity of the back muscles. Experimental results showed that the developed system significantly reduced back muscle activity during lifting range from 18 to 25 %, which is in line with those values found in previous studies on various back support exoskeletons [3]. Therefore, it can be concluded that the developed prototype has the effect of preventing LBP by assisting the worker during lifting. However, this study did not consider the influence of

the exoskeleton on the body kinematics, so biomechanical analysis will be conducted for more precise analysis of the system in future experiments. The developed prototype has a total weight of 9.2 kg (excluding battery), which meets the weight requirement (<10.5 kg) for portability and the battery (750 g) can power the system for 1.6 hour, which corresponds to 570 liftings at nominal frequency. However, it is expected that the weight of the system can be further reduced by optimizing and simplifying the system. Also, we will verify the system by measuring the metabolic energy expenditure of workers under a real working scenario in a dynamic working place.

In conclusion, by designing a portable pneumatic actuation system for a back support exoskeleton application, it is proposed that both portability and backdrivability can be achieved by applying the suggested design method to various pneumatic exoskeleton applications.

REFERENCES

[1] Ramos, Delfina G., Pedro M. Arezes, and Paulo Afonso. "Analysis of the return on preventive measures in musculoskeletal disorders through the benefit–cost ratio: A case study in a hospital." *International Journal of Industrial Ergonomics* 60 (2017): 14-25.W.-K. Chen, *Linear Networks and Systems* (Book style). Belmont, CA: Wadsworth, 1993, pp. 123–135.

[2] Zare, Mohsen, et al. "Evaluation of ergonomic approach and musculoskeletal disorders in two different organizations in a truck assembly plant." *International Journal of Industrial Ergonomics* 50 (2015): 34-42.

[3] De Looze, Michiel P., et al. "Exoskeletons for industrial application and their potential effects on physical work load." *Ergonomics* 59.5 (2016): 671-681.E. H. Miller, "A note on reflector arrays (Periodical style—Accepted for publication)," *IEEE Trans. Antennas Propagat.*, to be published.

[4] Aghilinejad, M.; Choobineh, A.R.; Sadeghi, Z.; Nouri, M.K.; and Bahrami Ahmadi, A., "Prevalence of Musculoskeletal Disorders Among Iranian Steel Workers," Iranian Red Crescent Medical Journal, Vol. 14, No. 4, 2012, pp. 198–203.

[5] Hoy, Damian, et al. "A systematic review of the global prevalence of low back pain." *Arthritis & Rheumatism* 64.6 (2012): 2028-2037.

[6] Innophys, "Muscle suit." [Online]. Available: https://innophys.jp/

[7] Cyberdyne, "Lumbar support.' [Online]. Available : https://www.cyberdyne.jp

[8] ATOUN, [Online]. Available : "http://atoun.co.jp

[9] Van Ninhuijs, B., et al. "Overview of actuated arm support systems and their applications." *Actuators*. Vol. 2. No. 4. Multidisciplinary Digital Publishing Institute, 2013.

[10] Veale, Allan Joshua, and Shane Quan Xie. "Towards compliant and wearable robotic orthoses: A review of current and emerging actuator technologies." *Medical engineering & physics* 38.4 (2016): 317-325.

[11] Rosales, I., et al. "Pneumatic assistant of one degree of freedom for lifting." *System Theory, Control and Computing (ICSTCC), 2015 19th International Conference on*. IEEE, 2015.

[12] Inose, Hiroki, et al. "Semi-endoskeleton-type waist assist AB-wear suit equipped with compressive force reduction mechanism." *2017 IEEE International Conference on Robotics and Automation (ICRA)*. IEEE, 2017.

[13] Parr, Andrew. *Hydraulics and pneumatics: a technician's and engineer's guide*. Elsevier, 2011.

[14] Wehner, Michael, et al. "Pneumatic energy sources for autonomous and wearable soft robotics." *Soft Robotics* 1.4 (2014): 263-274.

[15] Hong, Yun-Pyo, et al. "A Novel Pneumatic Generator with Pressure-Feedback Mechanism for Self-Injection of Hydrogen Peroxide." *IEEE/ASME Transactions on Mechatronics* 22.5 (2017): 1992-2002.

[16] Kim, Kyung-Rok, et al. "Design of a Compact Pneumatic Power Generator With a Self-Regulating Mechanism for Mobile Application." *IEEE/ASME Transactions on Mechatronics* 22.5 (2017): 1983-1991.

[17] Okui, Manabu, et al. "Hybrid Pneumatic Source Based on Evaluation of Air Compression Methods for Portability." *IEEE Robotics and Automation Letters* 3.2 (2018): 819-826.

[18] WU, Haifan, Ato KITAGAWA, and Hideyuki TSUKAGOSHI. "Development of a portable pneumatic power source using phase transition at the triple point." *Proceedings of the JFPS International Symposium on Fluid Power*. Vol. 2005. No. 6. The Japan Fluid Power System Society, 2005.

[19] Okui, Manabu, et al. "A pneumatic power source using a sodium bicarbonate and citric acid reaction with pressure booster for use in mobile devices." *Intelligent Robots and Systems (IROS), 2017 IEEE/RSJ International Conference on*. IEEE, 2017.

[20] Suzumori, Koichi, Akira Wada, and Shuichi Wakimoto. "New mobile pressure control system for pneumatic actuators, using reversible chemical reactions of water." *Sensors and Actuators A: Physical* 201 (2013): 148-153.

[21] Kim, Sangjoon J., et al. "Design of a Portable Pneumatic Power Source with High Output Pressure for Wearable Robotic Applications." *IEEE Robotics and Automation Letters* (2018).

[22] Bastien, Guillaume J., et al. "Effect of load and speed on the energetic cost of human walking." *European journal of applied physiology* 94.1-2 (2005): 76-83.

[23] Toxiri, Stefano, et al. "Using parallel elasticity in back-support exoskeletons: a study on energy consumption during industrial lifting tasks." *2019 Wearable Robotics Association Conference (WearRAcon)*. IEEE, 2019.

[24] Toxiri, Stefano, et al. "A parallel-elastic actuator for a torque-controlled back-support exoskeleton." *IEEE Robotics and Automation Letters* (2017).

[25] Toxiri, Stefano, et al. "A wearable device for reducing spinal loads during lifting tasks: Biomechanics and design concepts." *2015 IEEE International Conference on Robotics and Biomimetics (ROBIO)*. IEEE, 2015.

[26] Toxiri, Stefano, et al. "Rationale, implementation and evaluation of assistive strategies for an active back-support exoskeleton." (2018).

[27] Richer, Edmond, and Yildirim Hurmuzlu. "A high performance pneumatic force actuator system: Part I—Nonlinear mathematical model." *Journal of dynamic systems, measurement, and control* 122.3 (2000): 416-425.

[28] Chen, Baojun, et al. "A real-time lift detection strategy for a hip exoskeleton." *Frontiers in neurorobotics* 12 (2018): 17.

[29] Widia, Mirta, Siti Zawiah Md Dawal, and Nukman Yusoff. "Maximum acceptable frequency of lift for combined manual material handling task in Malaysia." *PloS one* 14.5 (2019): e0216918.

[30] Proportional pressure regulators (VPPM) technical datasheet, www.festo.com

[31] Hermens, Hermie J., et al. "Development of recommendations for SEMG sensors and sensor placement procedures." *Journal of electromyography and Kinesiology* 10.5 (2000): 361-374.

[32] Abdoli-E, Mohammad, Michael J. Agnew, and Joan M. Stevenson. "An on-body personal lift augmentation device (PLAD) reduces EMG amplitude of erector spinae during lifting tasks." *Clinical Biomechanics* 21.5 (2006): 456-465.

[33] Potvin, J. R., R. W. Norman, and S. M. McGill. "Mechanically corrected EMG for the continuous estimation of erector spinae muscle loading during repetitive lifting." *European journal of applied physiology and occupational physiology* 74.1-2 (1996): 119-132.